INTERNATIONAL JOURNAL FOR NUMERICAL AND ANALYTICAL METHODS IN GEOMECHANICS
Int. J. Numer. Anal. Meth. Geomech., **22**, 791–818 (1998)

NUMERICAL ANALYSIS OF THE MINIATURE PIEZOCONE PENETRATION TESTS (PCPT) IN COHESIVE SOILS

MURAD Y. ABU-FARSAKH[†], GEORGE Z. VOYIADJIS*[,‡] AND MEHMET T. TUMAY[§]

Louisiana State University, Baton Rouge, LA 70803-6405, USA

SUMMARY

An analytical model to simulate the penetration of the piezocone penetrometer in cohesive soils is presented here. The elasto-plastic coupled field equations of the saturated cohesive soils (given by Voyiadjis and Abu-Farsakh[1]) is used in this analysis. The numerical simulation of the piezocone penetration is implemented into a finite element program. The analytical model is used to analyze the miniature piezocone penetration tests (PCPT) conducted at LSU calibration chambers. Simulation of the piezocone penetration is done for two cases. In the first case, the soil–penetrometer interface friction is neglected, while in the second case, the soil–penetrometer interface friction is taken into consideration. The constraint approach is used to model the soil–piezocone interface friction in which the Mohr–Coulomb frictional model is used to define the sliding potential. Analysis is done for three different soil specimens with different stress histories. The results of the numerical simulations are compared with the experimental measurements of the miniature piezocone penetration tests (PCPT) in cohesive soil specimens conducted in LSU calibration chambers. The resulting excess pore pressure distribution and its dissipation using the numerical model are compared with some available prediction methods. © 1998 John Wiley & Sons, Ltd.

INTRODUCTION

There is an increased concern recently towards the evaluation of different engineering soil parameters (e.g. geotechnical parameters, flow characteristics, etc.) using *in situ* testing. The piezocone penetrometer is one of the most widely used for *in situ* investigations and soil exploration. The piezocone penetrometer is capable of measuring the cone tip resistance, sleeve friction, and pore pressures simultaneously. These measurements can be effectively utilized for soil profiling and identification. The dissipation data can be used to evaluate the flow and consolidation characteristics of soils. Interpretation of the PCPT data is a complex task since it is affected by many variables[2, 3] including piezocone design, testing procedures and soil characteristics. Location and size of the pore pressure element also influence the magnitude of the measured pore pressure[2] especially in overconsolidated stiff clays, where a large pore pressure

*Correspondence to: G. Z. Voyiadjis, Louisiana State University, Baton Rouge, LA 70803-6405, U.S.A.
[†]Research Associate, LTRC
[‡]Boyd Professor, Department of Civil and Environmental Engineering
[§]Professor and Director of Research, LTRC

Contract grant sponsor: National Science Foundation; contract grant number: MSS-9312707; contract grant sponsor: Louisiana Transportation Research Center; contract grant number: Task Order No. 736-99-0293

CCC 0363–9061/98/100791–28$17.50

Received 2 February 1997
Revised 24 November 1997

gradient develops around the tip.[4–6] Several interpretation procedures have been used to analyze piezocone penetration and to evaluate some engineering soil parameters. These procedures are usually based either on the bearing capacity theories[7] or the cavity expansion theories.[8–10] The strain path method,[11, 12] semi-empirical methods[13] and dislocation method[14] have been used in the cavity expansion analysis. Kiousis *et al.*,[3] used the finite element technique to analyze the cone penetration assuming a pre-bored hole to a certain depth with zero initial *in situ* stresses. A combination of a strain path method with the finite element technique have been proposed by Teh and Houlsby.[15] Most of the methods that are based on the cavity expansions assume that the soil around the cone follows a certain deformation pattern that is different from the real displacement field of the soil elements resulting from piezocone penetration.[3] In addition, the cavity expansion theory cannot correctly model the strain paths followed by the soil element[11] during cone penetration with the resulting stresses are not necessary in equilibrium, and also does not distinguish between the different soil deformation modes due to different cone geometries. Moreover, very little work has been done that include the large deformation finite strain behaviour of the soil. The soil–piezocone interface friction is usually neglected in most models. Strains are reported to exceed 100 per cent.[12, 3] The piezocone penetration test results depend on many factors, e.g. soil type and compressibility characteristics, stress history and the presence of fissures and cracks. The presence of fissures and cracks in the soil deposit tend to increase the *in situ* hydraulic conductivity and coefficient of consolidation. To analyze accurately the piezocone penetration test (PCPT), it is necessary to have a numerical model that takes into consideration the large deformation of the soil around the tip, non-linear soils behaviour, changing of the boundary condition with penetration and the soil–piezocone interface friction. To validate the numerical model it is necessary to compare it with controlled laboratory calibration tests of known soil types, characteristics and stress history.

This paper presents an analytical model to analyze the miniature piezocone penetration in cohesive soils. In this analysis, the elasto-plastic coupled field of the saturated cohesive soils as given by Voyiadjis and Abu-Farsakh[1] is used. Formulation of these equations is based on the theory of mixtures for inelastic porous media for large deformations, finite strains in an updated Lagrangian reference frame. The modified Cam-clay model is adopted to describe the plastic behavior of the clayey soil. The penetration of the piezocone penetrometer in cohesive soils is numerically simulated and implemented in the finite element program. The continuous penetration of the piezocone is simulated by imposing an incremental vertical displacement to the cone tip boundaries. The problem is treated as a boundary problem that includes changing of the boundary condition as penetration proceeds incrementally. The constraint approach is used in this study in order to model the soil–piezocone interface friction in which the Mohr–Coulomb frictional model is used to define the sliding potential.

The results of the numerical simulation are compared with experimental laboratory measurements of the miniature piezocone penetration tests (PCPT) conducted at Louisiana State University Calibration Chamber (LSU/CALCHAS).[16, 2] Tests were performed for different soil specimens with different stress histories including isotropic normally consolidated, overconsolidated and K_0-anisotropic consolidated soil specimens. The cone tip resistance and excess pore pressure profiles with penetration and the developed strain, stress and excess pore pressure fields around the piezocone are presented. The resulting excess pore pressure distribution and its dissipation are compared with the predictions of some available methods.

ANALYTICAL MODEL OF THE PIEZOCONE PENETRATION

The piezocone penetration analysis is treated as an axi-symmetric boundary value problem with the need of changing the boundary conditions as the piezocone penetrometer advances. In the simulation, the piezocone penetrometer is assumed to be infinitely stiff and no tensile stresses are allowed to develop along the centreline boundaries. Because the soil around the cone undergoes substantial displacement during penetration, a large deformation finite strain formulation is used in the analysis of this problem. For numerical purposes, the piezocone penetrometer is assumed to be initially pre-bored to a certain depth with the initial stresses remaining unchanged. If one attempts to initiate the analysis by starting the penetration from the top surface of the soil, one will encounter tremendous computational difficulties involved in the transient state due to large rotations of the elements involved. In order to avoid the accumulation of associated errors in the final analysis, one has to start the penetration from a pre-bored depth. This causes an error in the initial stresses involved. In order to minimize such errors, the pre-bored depth is kept to a minimum of 20 mm in this case.

The numerical simulation is performed for two cases. The first case, the soil–penetrometer interface friction is assumed to be negligible. In the second case, the soil–penetrometer interface friction coefficient is taken as 0·25, which corresponds to an angle of friction $\delta = 14^\circ$ between the soil and the piezocone surface. The continuous penetration of the piezocone is simulated by applying an incremental vertical displacement of the cone boundary as shown in Figure 1. The vertical displacement (penetration) is applied at the rate of 2 cm/s, which is the same rate used in the piezocone penetration experiment.

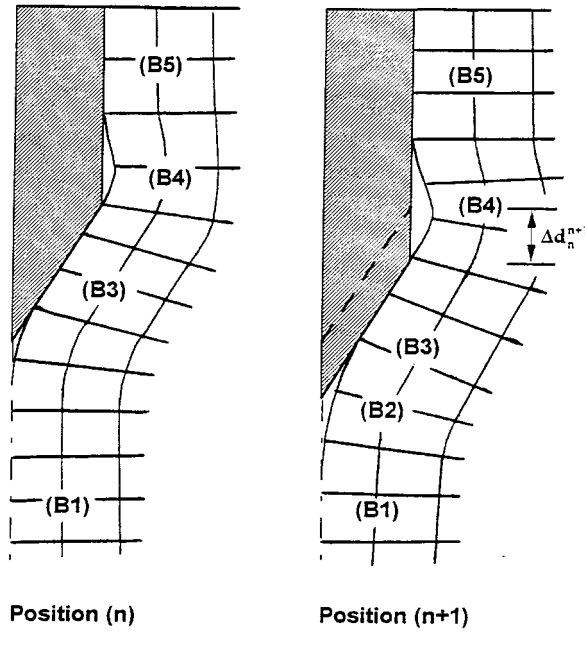

Figure 1. Incremental penetration of the piezocone penetrometer

Boundary conditions change

In *Case* 1, where the interface friction is neglected, the nodes along the inclined conical surface of the cone and along the piezocone shaft are allowed to slide along the boundary from the beginning of the first incremental penetration. During the incremental penetration, the nodes along the boundary are continuously checked and their boundary conditions are appropriately adjusted. Based on the previous boundary condition at load increment $(k-1)$, a new boundary condition state is assumed for the load increment (k), depending on the load and displacement criteria. The validity of the assumed trial boundary condition is tested before one proceeds to the next loading increment. Table I summarizes the decision matrix for selecting the new nodal boundary condition. For example, when tension occurs ($F_n^k < 0$) in any of the nodes along the centreline boundary below the cone tip (boundary type B1), the node is released and allowed to move freely while its boundary condition becomes a B2 type. The free nodes of type B2 are allowed to move freely until they reach the cone trip boundary ($Y_n > Y_{\text{tip}}$). Their movement is then restricted along the skew conical surface of the cone and its boundary changes to B3 type boundary. Once the horizontal coordinates of any node of type B3 boundary condition exceed the penetrometer radius ($X_n > r_0$), the node is then released and allowed to move freely and its boundary is changed to B4 type. Once the free nodes of B4 boundary return back to the penetrometer shaft boundary ($X_n < r_0$), they are then restricted from any further movement in the horizontal direction and allowed only to slide vertically along the cone shaft as indicated by B5 boundary type. If for some reason, tension occurs for any node of boundary type B5, this node will be freed again and its boundary is changed to B4 type.

In *Case* 2, the soil–piezocone interface friction is included. During the piezocone penetration, the element nodes along the centreline (boundary types B1 and B2) get into contact with the piezocone boundary surface in sequence, rather than simultaneously. In addition, the penetration of the piezocone at a rate of 2 cm/s makes it difficult to use interface elements between the soil and piezocone surface, due to the fact that the interface elements cannot be stretched to infinity. Therefore, a simple constraint approach at the nodal level, similar to the interface model proposed by Katona,[17] is adapted in this study in order to account for the soil–penetrometer interface friction, as described later. At the beginning of penetration, all the nodes along the inclined conical surface and along the piezocone shaft are prevented from sliding along the surface and are forced to move vertically with the cone boundary incremental movement until the sliding potential occurs. The sliding potential is reached, when the tangent frictional forces (F_t) of the nodes along the boundary surface reach the allowable friction forces ($F_t > F^s$), as described

Table I. Decision matrix for changing nodal boundary condition

Load step	(k) 1	2	3	4	5
$(k-1)$					
1	$F_n > 0$ and $Y_n < Y_{\text{tip}}$	$F_n < 0$ (tension)	$Y_n > Y_{\text{tip}}$		
2	$X_n < 0$	$X_n > 0$ and $Y_n < Y_{\text{tip}}$	$Y_n > Y_{\text{tip}}$		
3			$X_n < r_0$	$X_n > r_0$	
4				$X_n > r_0$	$X_n < r_0$
5				$F_n < 0$	$F_n > 0$

later. Following that, these nodes are allowed to slide along the skew surface and along the cone shaft surface. The changes of the boundary conditions for case 2 are similar to those of case 1 except for the consideration of interface friction. When the nodes of boundary types B2 and B4 reach the boundary surface, these nodes are initially fixed and vertically displaced until the sliding potential is reached. They are then allowed to slide along the skew boundary surface. The allowable interface friction (F^s) for each node at the boundary, is calculated at the end of each increment.

THE FRICTIONAL INTERFACE MODEL

There are several approaches available in the literature to model the interface friction. Zienkiewicz *et al.*[18] used a continuous solid elements as interface elements with a simple non-linear material property for shear and normal stresses, assuming uniform strain in the thickness direction. Katona[17] and Lei *et al.*[19] used the constraint approach with the principle of virtual work to derive an interface model. Goodman *et al.*[20] introduced a zero-thickness interface element. The element formulation is derived on the basis of relative nodal displacements of the solid elements adjacent to the interface element. In recent years, a number of investigators have considered the use of thin-layer interface elements, e.g. Desai *et al.*,[21] and Sharma and Desai.[22] In this study, a simple constraint approach similar to the one proposed by Katona[17] is used to model the soil–piezocone interface friction. During the piezocone penetration, three interface states can be identified: fixed, slip and free states. The Mohr–Coulomb frictional model is used to define the sliding potential for the fixed state. Thus, the maximum allowable interface tangent frictional force, F^s at the end of increment k is given by

$$F^s = F_a^k + F_n^k \tan\delta \tag{1}$$

where F_a^k is the soil–piezocone adhesion force at load increment k, F_n^k is the normal effective force at load increment k, and δ is the angle of friction between the soil and the piezocone surface. Solution for the new nodal interface state has to be determined iteratively, whereby a particular state (fixed, slip or free) is assumed and solved to obtain a trial solution. The trial solution is then used to check whether the assumed trial state is correct, and if not, which state is more likely to be correct. At the same time, the trial state is used to obtain the new nodal loads and displacements. Table II describes the decision matrix for selecting a new interface state during iteration within each load increment given the previous interface state and the load–displacement criteria. The specified values for the constraint load and displacement is described in Table III. For example, if the previous interface state was fixed, then we need to determine if the effective normal force F_n^k is

Table II. Decision matrix for selecting new interface state

Iteration	(i) Fix	Slip	Free
$(i-1)$			
Fix	$F_n > 0$ and $F_t < F^{s**}$	$F_n > 0$ and $F_t < F^{s**}$	$F_n < 0$ (tension)
Slip	$F_n > 0$ and $\Delta u_s \cdot F^s < 0$	$F_n > 0$ and $\Delta u_s \cdot F^s < 0$	$F_n < 0$ (tension)
Free	$\Delta u_n < 0$		$\Delta u_n > 0$

** $F^s = F_a + F_n \tan\delta$

Table III. Specified values for constraint nodal loads and displacements

Load step	(k) Fix	Slip	Free
($k-1$)			
Fix	$d_n = 0$	$d_n = 0$	$N = -F_n^{k-1}$
	$d_s = 0$	$T = F^s - F_t^{k-1}$	$T = -F_t^{k-1}$
Slip	$d_n = 0$	$d_n = 0$	$N = -F_n^{k-1}$
	$d_s = 0$	$T = F^s - F_t^{k-1}$	$T = -F_t^{k-1}$
Free	$d_n = -\Delta_n^{k-1}$	$d_n = -\Delta_n^{k-1}$	$N = 0$
	$d_s = \Delta u_n(\Delta_s/\Delta_n)$	$T = F^s$	$T = 0$

compressive and if the tangent interface force F_t is less than the maximum allowable frictional force F^s. If not, the fixed interface state is not correct, and the new interface state is slip or free depending on whether F_n^k is tensile or compressive. Row 3 in Table II implies that the slip state cannot be reached directly from the free state and instead it has to be reached by iterative path; the free to fix to slip.

SOIL SPECIMENS: DESCRIPTION AND MODELLING PARAMETERS

In this work the analysis is done for a miniature piezocone penetrometer of an area of 1 cm^2 and a standard cone apex angle of 60°, which is of the same size as the piezocone used in the LSU/CALCHAS tests.[2,16]

The results of the numerical simulation are compared with the miniature piezocone penetration tests (PCPT) conducted on cohesive soil specimens prepared at LSU/CALCHAS. The soil is prepared by mixing kaolinite and fine sand ($D_{60}/D_{10} = 1{\cdot}4$) at a water content of twice the liquid limit. A mixture of 50 per cent kaolinite and 50 per cent Edgar fine sand by weight is used to prepare the K-50 specimens. The K-50 soil specimen has a liquid limit $w_L = 30$ per cent and a plastic limit, $w_p = 16$. The specimens are consolidated against a backpressure of 138 kPa. Full details of specimen preparation, test procedure and type of penetrometer used are found in Kurup *et al.*[2] and Voyiadjis *et al.*[16] Summary of the stress history of the soil specimens 1, 2 and 3 is presented in Table IV. The filter used to measure the pore-water pressure is located either in the lowest 1/4 of the cone at the very tip (U1 configuration) or starting 0·5 mm above the base of the cone with 2 mm vertical height (U2 configuration). A summary of the piezocone penetration tests is presented in Table V.

The modified Cam clay model is used in this study in order to describe the plastic behaviour of soil. The yield locus for the modified Cam clay is given by

$$f(P, q, P_c(\varepsilon_v^p) \equiv M^2P^2 - M^2P_cP + q^2 = 0 \tag{2}$$

which represents an ellipse in the P–q plane. In equation (2), P and q are the mean effective and deviatoric stresses respectively, P_c is the strain-hardening parameter representing the apex of the yield locus ellipse in the P-axis. If $P \geqslant P_c/2$, the model is either in the strain-hardening region or at the critical state. If $P < P_c/2$, the model is in the strain-softening region which is not suitable for application here and has numerical difficulties.[23,24] To overcome the numerical difficulty in the treatment of the strain-softening region ($P < P_c/2$), one can introduce a perfectly plastic idealization that is compatible with the modified Cam clay model. One can use the critical state line as a perfectly plastic yield surface of the extended von Mises type. Another approach can be used by

Table IV. Summary of the stress history of the soil specimens[25]

Specimen no.	Soil type	Chamber consolidation	OCR	Final effective stress (KPa)	
				Vertical	Hortizontal
1	K-50	Isotropic	1	207	207
2	K-50	Isotropic	5	41·4	41·4
3	K-50	K_0-anisotropic	1	207	107·6

Table V. Summary of piezocone penetration tests[25]

Specimen no.	Test	Filter location	
		U1 configuration	U2 configuration
1	PCPT1		Yes
	PCPT2	Yes	
2	PCPT3		Yes
	PCPT4	Yes	
3	PCPT5		Yes
	PCPT6	Yes	

treating the modified Cam clay yield surface in the strain-softening region as a perfectly plastic yield surface.[23] In this study, the second approach is used.

The soil parameters for the K-50 specimens used here for the modified Cam clay model are: the slope of the virgin consolidation line in e–$\ln P$ space, $\lambda = 0{\cdot}11$; the slope of the unloading–reloading line in the e–$\ln P$ space, $\kappa = 0{\cdot}0240$; the slope of the critical state line, $M = 1{\cdot}2$; $\Gamma = 1{\cdot}162$; the coefficient of permeability for the soil, $K = 0{\cdot}5 \times 10^{-9}$ m/s; and the Poisson's ratio $\nu = 0{\cdot}3$. These parameters are taken from Kurup.[25] An anisotropic soil model (which is under developing now) will be used in the future work in order to better correlate with the material behaviour of specimen 3.

ANALYSIS AND VERIFICATION OF THE FINITE ELEMENT SIMULATION

A number of different finite element meshes, with different degrees of refinement, were tried first in order to obtain the appropriate mesh for the analysis of the piezocone penetration problem that satisfies convergence to a unique solution. The finite element mesh used in this analysis is presented in Figure 2. The eight-node isoparametric finite element, Q8P4, is used in this analysis.

Cone tip resistance profiles

The cone tip resistance q_c, at any penetration depth, can be estimated by integrating the vertical stress components of the element faces along the cone tip. The calculated cone tip resistance profiles during the piezocone penetration for the two cases (with and without interface friction) are compared with those obtained experimentally from the PCPT as shown in Figure 3.

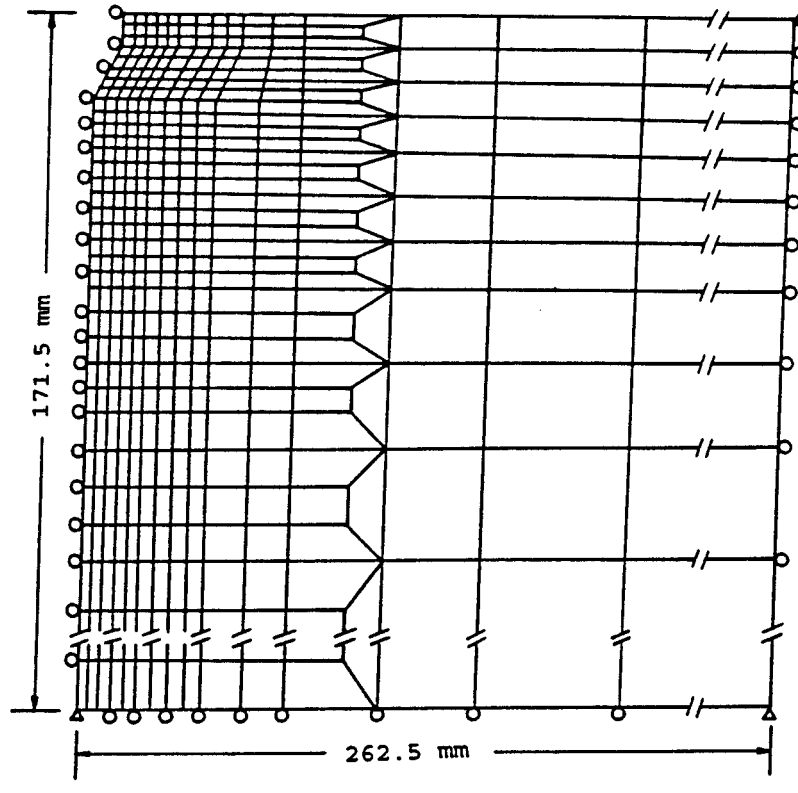

Figure 2. Finite element mesh of the piezocone penetration problem

It can be seen that the cone tip resistance computed numerically increases rapidly until it reaches a steady state condition at a depth ranging from 20 to 30 mm. The calibration chamber tests usually take the 'steady-state' value as a single measurement. It is however, noticed that the computed cone tip resistance develops at a faster rate than those obtained experimentally. The variation may be due to some boundary effects and/or saturation difficulties in the experimental procedure near the top surface of the soil specimen; and also due to prestressing problems. This can be noticed if one compares the cone tip resistance obtained, for the same specimen, at two different filter locations. The final values obtained from the numerical model after the steady state condition is reached are close to those obtained experimentally. Stress values obtained assuming soil–penetrometer interface friction $\mu = 0{\cdot}25$, give higher cone tip resistance compared to those in which the interface friction is neglected. The difference ranges from about 10 per cent for Ko-anisotropic consolidated specimen 3 to about 15 per cent for the normally consolidated specimen 1.

Excess pore pressure profiles

The developed excess pore pressure profiles during piezocone penetration obtained numerically are compared with those obtained experimentally from the PCPT for both U1 and U2

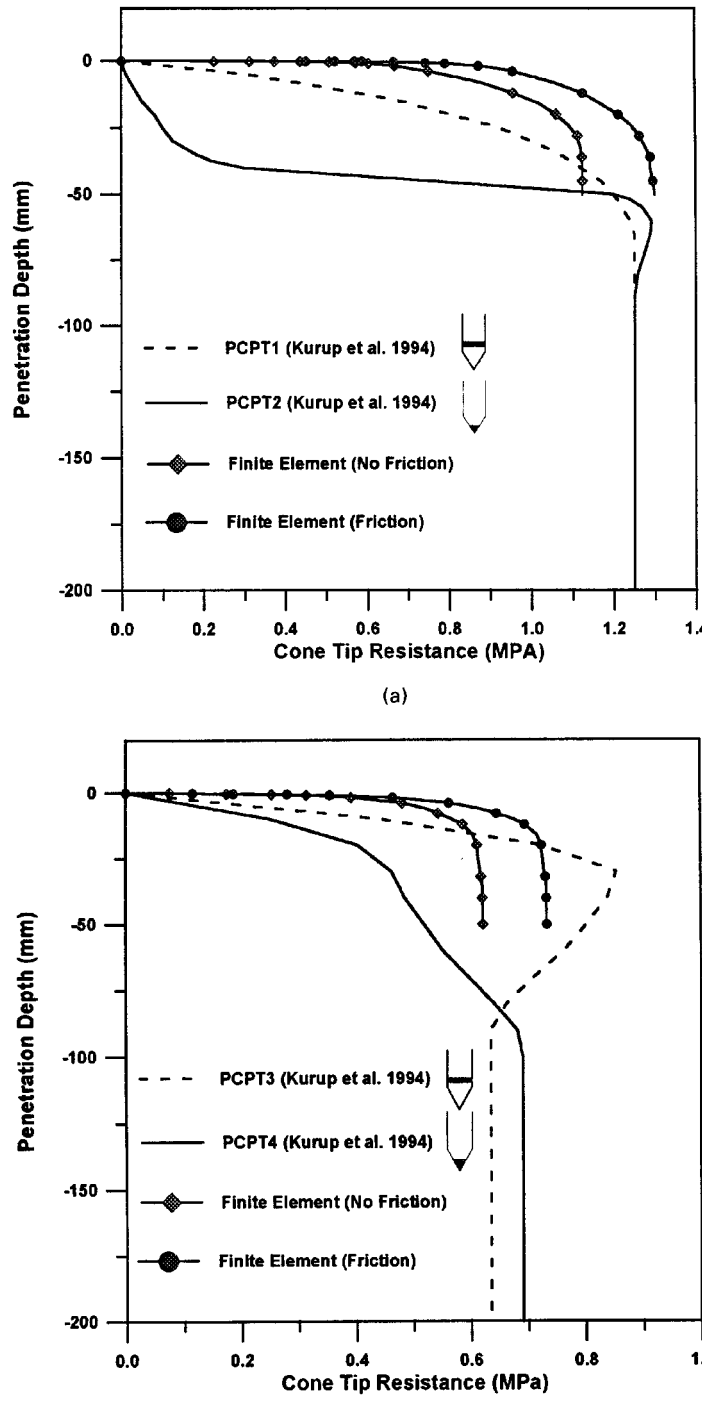

Figure 3. Cone resistance profiles during piezocone penetration: (a) specimen 1, (b) specimen 2, and (c) specimen 3

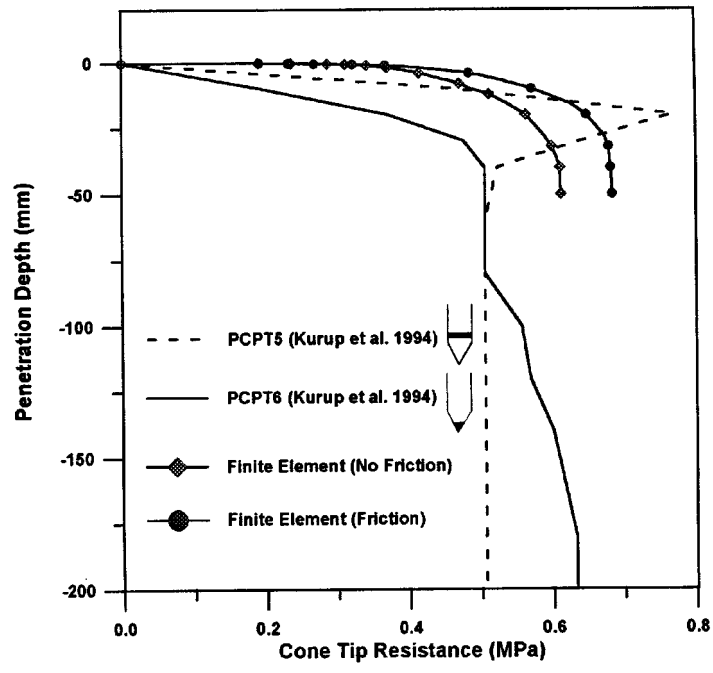

Figure 3. (Continued)

configurations as shown in Figures 4–6 for specimens, 1, 2, and 3, respectively. The developed excess pore pressures obtained numerically (for U1 and U2 configurations) increase rapidly until they reach a steady-state condition at a depth of 20–30 mm. They also develop at a faster rate than those obtained experimentally. This behaviour is similar to that obtained for the cone resistance profiles. The difference can be attributed to some boundary effects and/or saturation difficulties near the top surface of the soil specimen in the experimental set-up. The final excess pore pressures at the steady-state condition are quite close to those obtained experimentally. It is interesting to note that a negative excess pore pressure is likely to develop near the cone base (U2 configuration) at the early stages of the penetration due to the soil–piezocone separation near the cone base. The effect of the soil–penetrometer interface friction is more obvious for the U1 configuration than it is for the U2 configuration. The excess pore pressure deviates by (10–15 per cent) due to the interface friction. This is expected since the soil is subjected to more local shearing and consequently, the contribution of the shear-induced excess pore pressure will affect the total excess pore pressure.

Stress field

The contours of the effective radial (σ'_r), axial (σ'_z), tangantial (σ'_θ), and shear stresses (τ_{rz}) around the piezocone penetrometer at a penetration depth of 25 mm for specimen 1 and for case 1 are presented in Figure 7. The initial stress state for the specimen is isotropic with

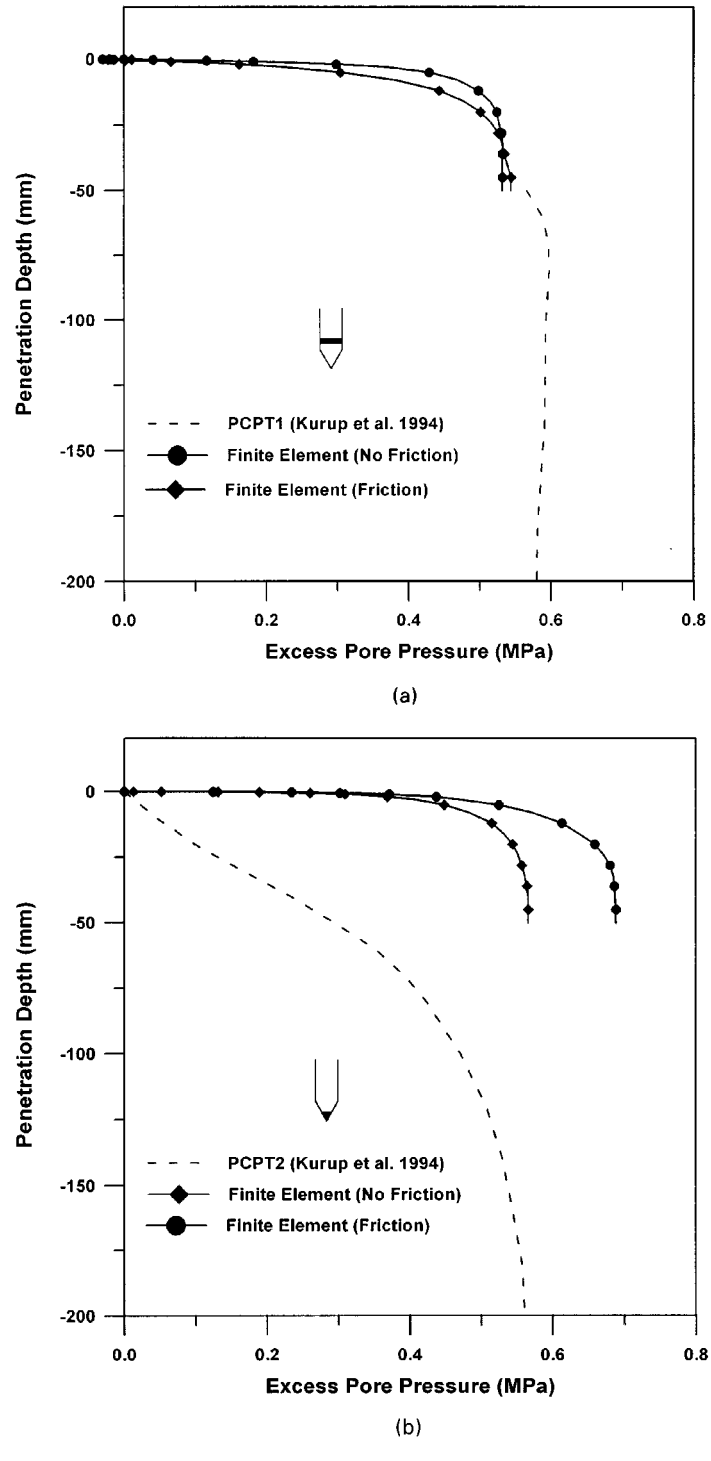

Figure 4. Excess pore pressure profiles during piezocone penetration for specimen 1: (a) at the cone base, (b) at the cone tip

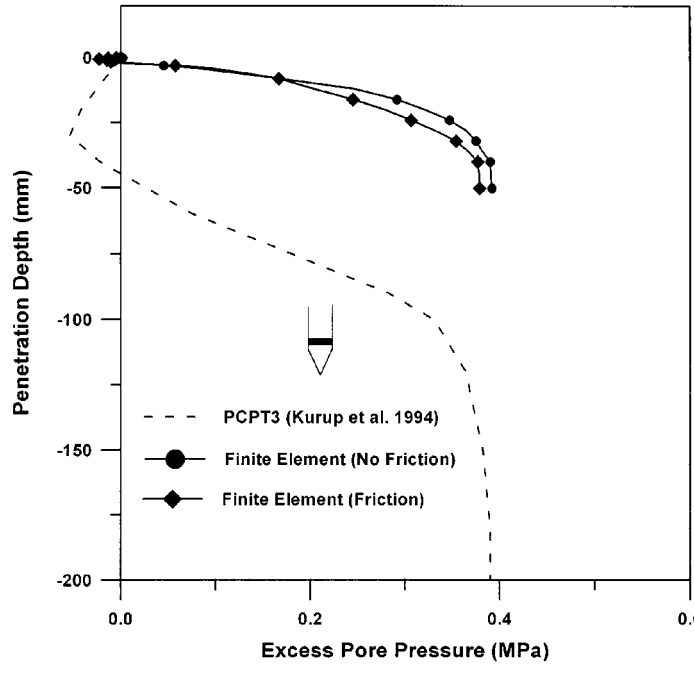

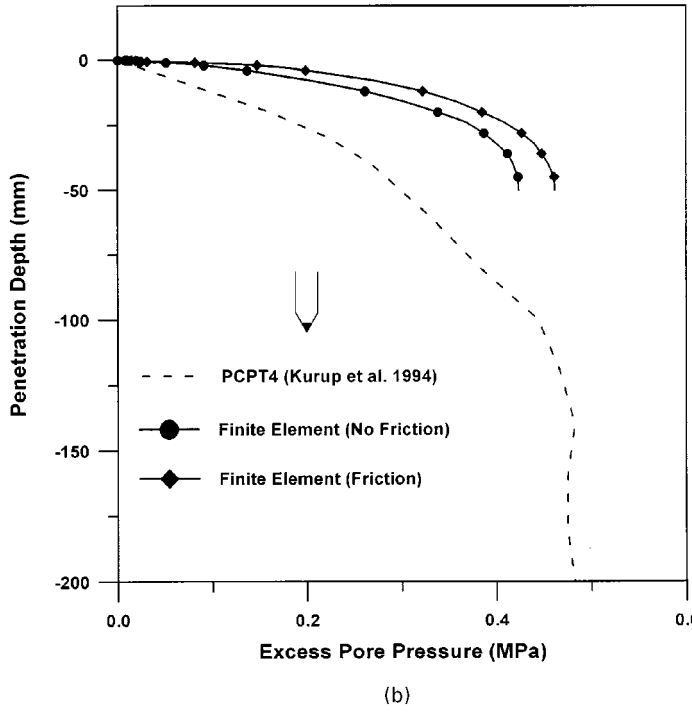

Figure 5. Excess pore pressure profiles during piezocone penetration for specimen 2: (a) at the cone base, (b) at the cone tip

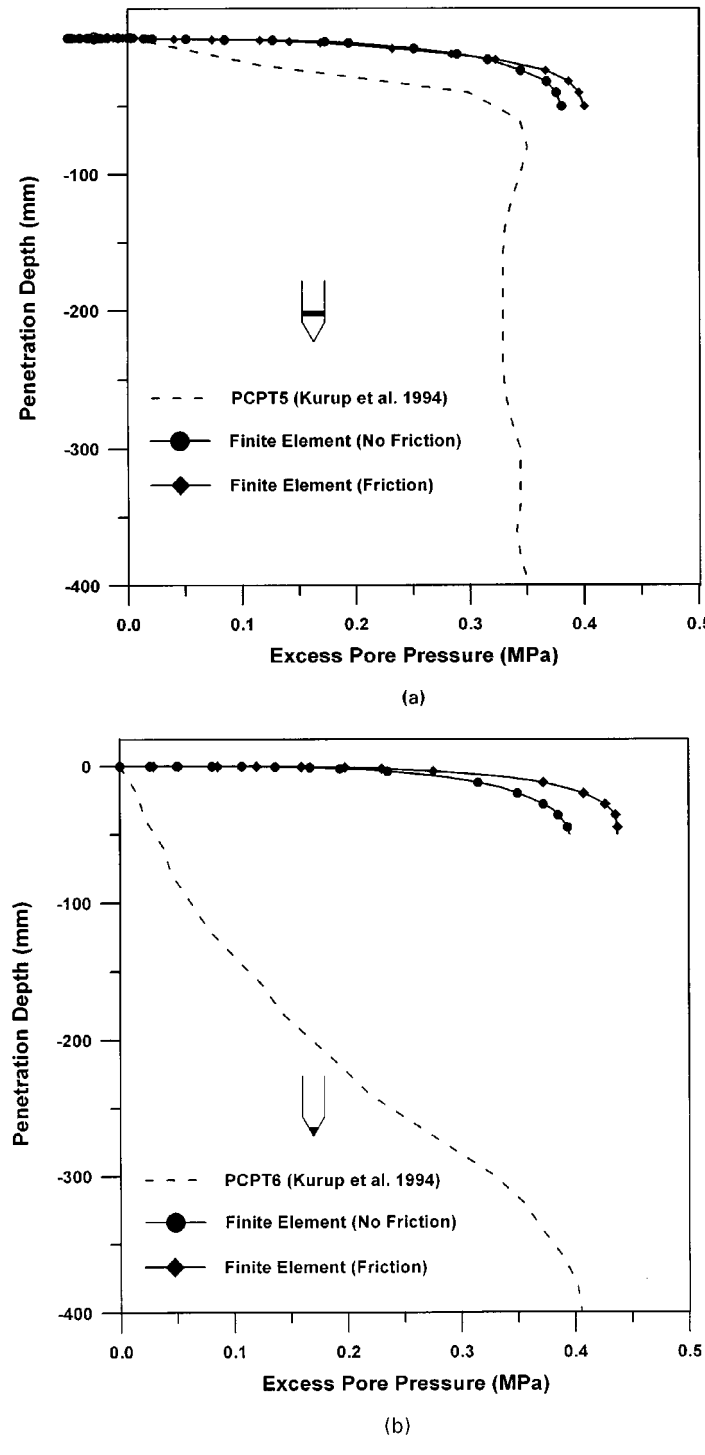

Figure 6. Excess pore pressure profiles during piezocone penetration for specimen 3: (a) at the cone base, (b) at the cone tip

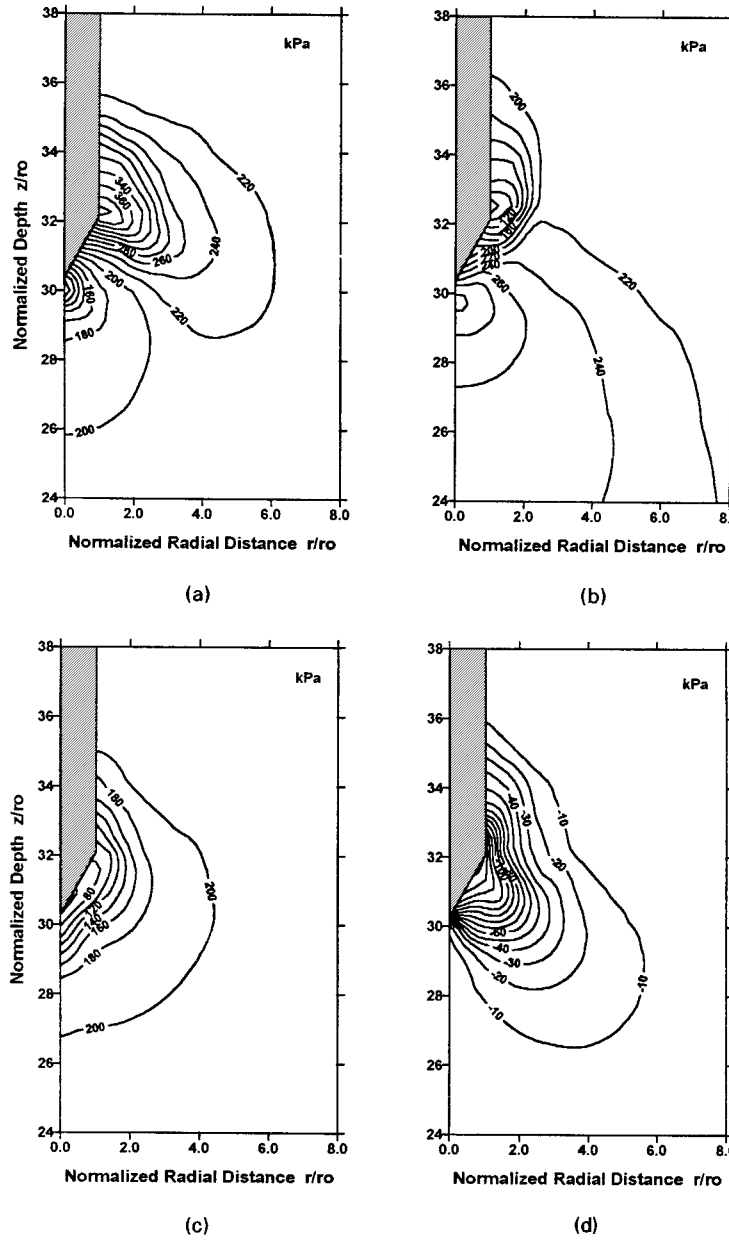

Figure 7. Contours of stresses around the piezocone penetrometer of specimen 1, case 1, for penetration of 25 mm: (a) radial effective stress, σ'_r, (b) axial effective stress, σ'_z, (c) tangential effective stress σ'_θ, and (d) shear stress, τ_{rz}

$\sigma'_r = \sigma'_z = \sigma'_\theta = 207$ kPa. The radial effective stress (σ'_r) around the piezocone penetrometer increases in the region above the midpoint of the cone tip up to 424 kPa immediately above the cone base. However, it drops to 48 kPa below the cone tip as shown in Figure 7(a). The axial effective stress (σ'_z), arising from the 25 mm penetration, increases in the region below the cone face

up to 306 kPa below the cone tip, and decreases in the region above the cone face to 62 kPa as shown in Figure 7(b). The effective tangential stress (σ'_θ) around the piezocone decreases radially from 207 kPa (initial stress) to 43 kPa at the lower-half of the cone face as shown in Figure 7(c). The maximum shear stress (τ_{rz}) induced is -166 kPa. The shape of the shear stress distribution around the piezocone is a bulb with the maximum value located at the cone face and oriented at an angle of approximately 45° to the cone face. The shear stress bulb is also extended behind the cone face. Figures 8, 9, and 10 represent contours of octahedral shear stress (τ_{oct}) induced by 25 mm penetration depth for specimens 1, 2, and 3, respectively. The octahedral shear stress is a measure of the resulting shearing in the soil specimen. The change in octahedral shear stress is important in the generation of excess pore pressure around the piezocone. The excess pore pressure developed during the piezocone penetration can be expressed as a function of the change of the mean effective stress and the octahedral shear stress through the following relationship:

$$\Delta u = \Delta\sigma_{oct} + \alpha\Delta\tau_{oct} \tag{3}$$

The maximum octahedral shear stress is concentrated around the upper portion of the conical face for case 1 (neglecting interface friction); while for case 2 (interface friction), it is concentrated around both the upper and lower portions of the conical face. It is to be noted that the affected shearing zone for the overconsolidated specimen is localized in a smaller zone than the other two specimens. Similar behaviour is obtained in the excess pore pressure distribution as will be discussed later.

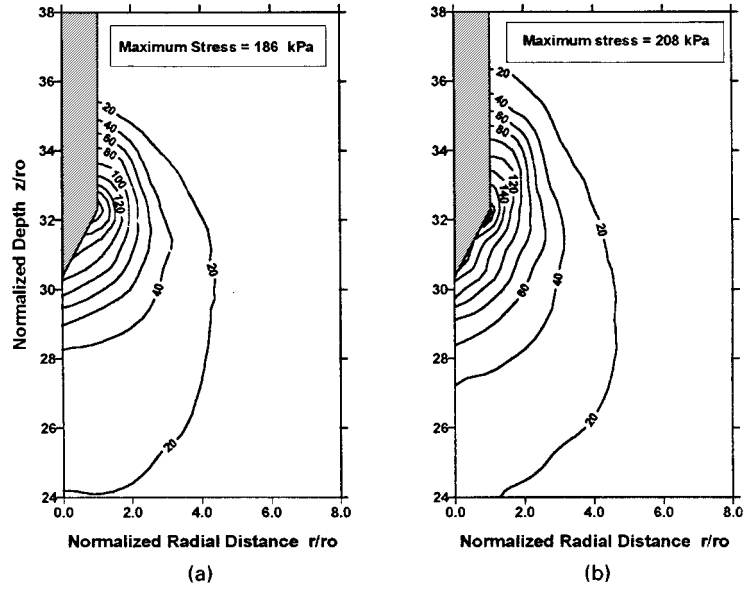

Figure 8. Contours of octahedral shear stress, τ_{oct}, around the piezocone penetrometer of specimen 1 for penetration of 25 mm: (a) $\mu = 0$, (b) $\mu = 0{\cdot}25$

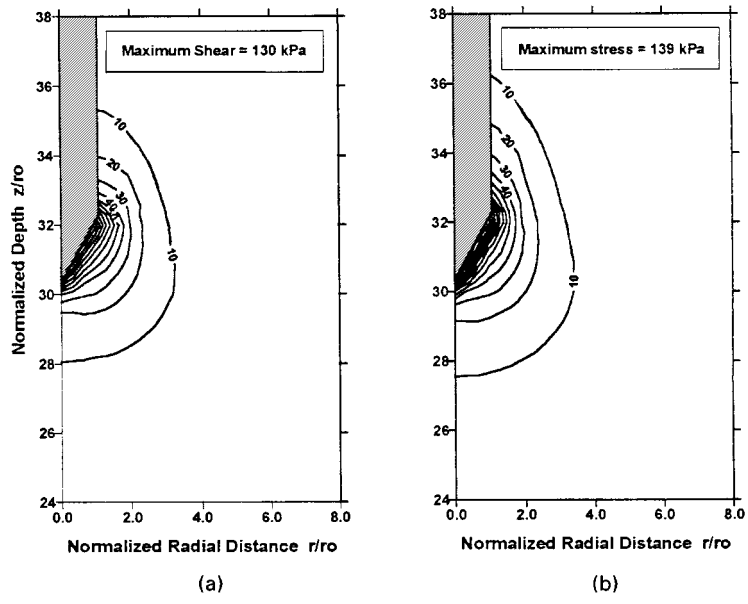

Figure 9. Contours of octahedral shear stress, τ_{oct}, around the piezocone penetrometer of specimen 2 for penetration of 25 mm: (a) $\mu = 0$, (b) $\mu = 0{\cdot}25$

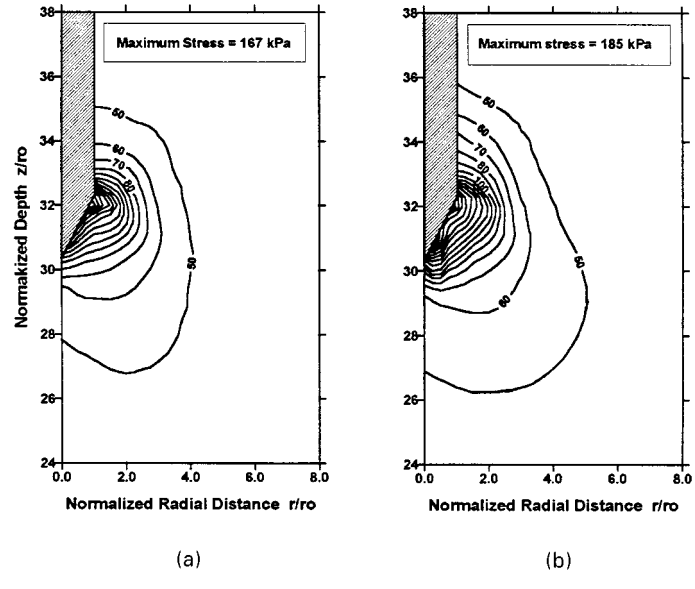

Figure 10. Contours of octahedral shear stress, τ_{oct}, around the piezocone penetrometer of specimen 3 for penetration of 25 mm: (a) $\mu = 0$, (b) $\mu = 0{\cdot}25$

Spatial excess pore pressure distribution

The spatial distribution of the excess pore pressure developed around the piezocone penetrometer at a penetration depth of 25 mm is shown in Figures 11–13 for specimens 1, 2, and 3, respectively. It can be seen that the maximum concentration of the excess pore pressure for case 1 when the soil–penetrometer interface friction is neglected ($\mu = 0$), is located around the upper-third of the cone as shown in Figures 11(a), 12(a) and 13(a). For case 2 with the coefficient of interface friction $\mu = 0{\cdot}25$, the maximum concentration of the excess pore pressure is located around the lower third of the cone as shown in Figures 11(b), 12(b) and 13(b). A possible negative pore pressure is likely to develop, especially for the overconsolidated specimen, behind the cone base due to the soil–piezocone separation. This produces a large pore pressure gradient just behind the cone base which makes the excess pore pressure measurement in this region (as in U2 configuration) highly sensitive to the pore element location, especially for overconsolidated soils.

The excess pore pressures developed around the cone due to piezocone penetration are localized in a very small region surrounding the cone face especially for the overconsolidated soils. The 50 kPa contour line extends to about $6r_0$, $3r_0$, and $4r_0$ for the isotropic normal consolidated, isotropic overconsolidated, and K_0-anisotropic consolidated specimens, respectively. The distribution of the spatial excess pore pressures resulting from the proposed elasto-plastic finite element analytical model and its corresponding dissipation are compared with the cavity expansion method proposed by Tortensson[8,9] and Vesic,[10] the semi-empirical methods given by Gupta and Davidson,[13] and the strain path method given by Levadoux and Baligh,[12] and Teh and Houlsby[15] as shown in Figures 14–16 for specimens 1, 2, and 3, respectively. Table VI

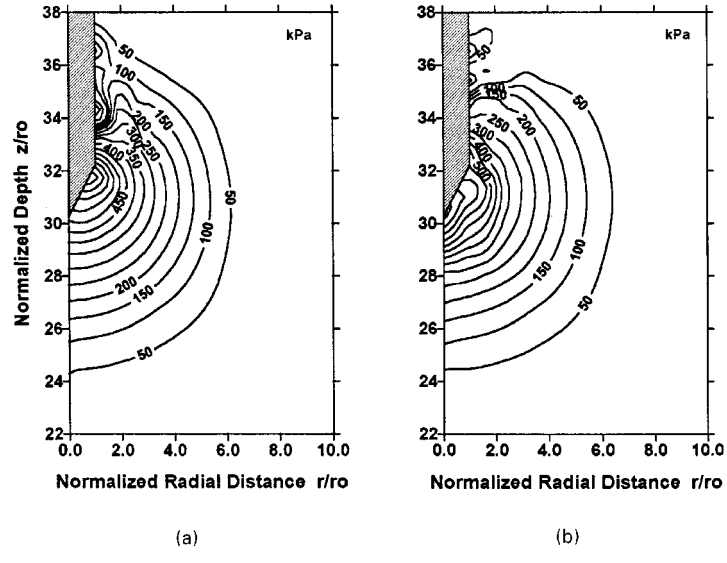

Figure 11. Contours of excess pore pressures around the piezocone penetrometer for penetration of 25 mm of specimen 1: (a) $\mu = 0$, (b) $\mu = 0{\cdot}25$

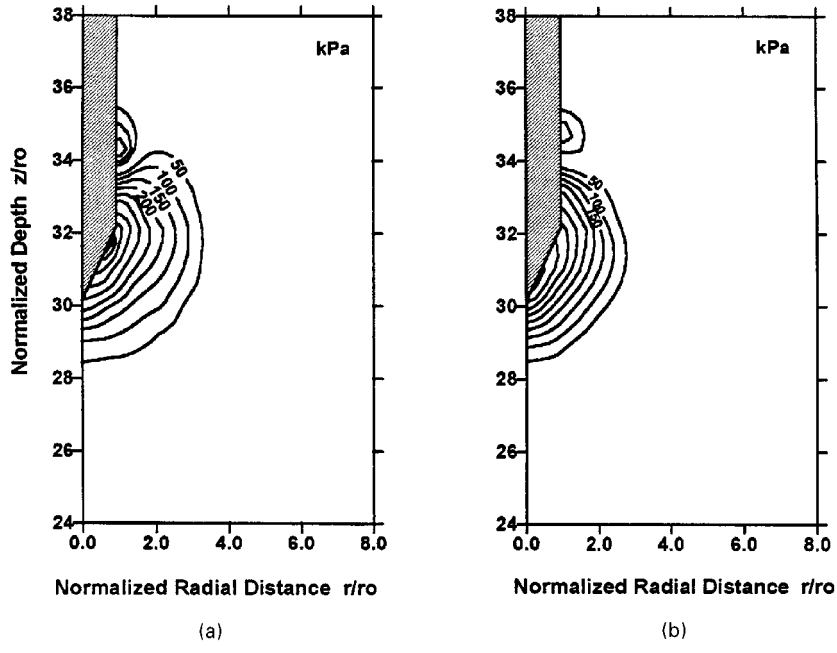

Figure 12. Contours of excess pore pressures around the piezocone penetrometer for penetration of 25 mm of specimen 2: (a) $\mu = 0$, (b) $\mu = 0{\cdot}25$

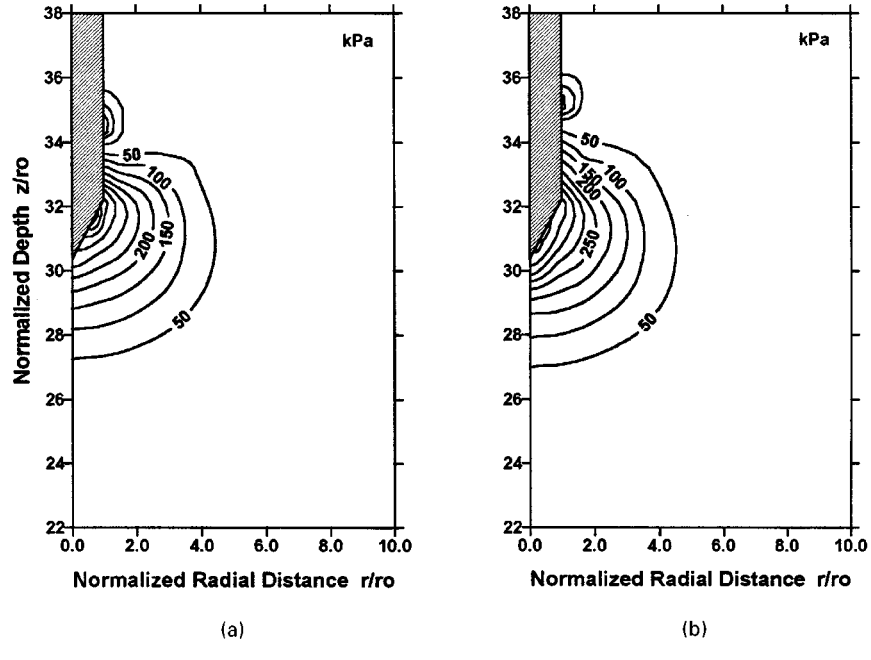

Figure 13. Contours of excess pore pressures around the piezocone penetrometer for penetration of 25 mm of specimen 3: (a) $\mu = 0$, (b) $\mu = 0{\cdot}25$

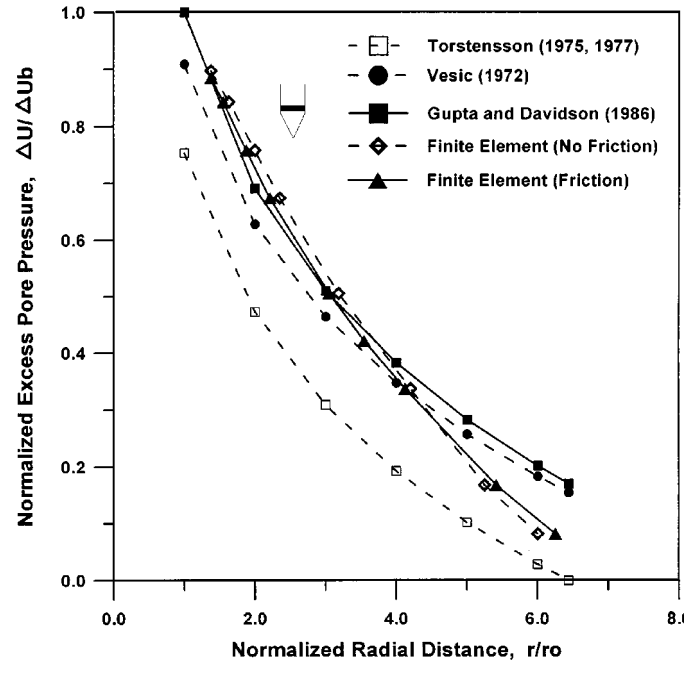

(a)

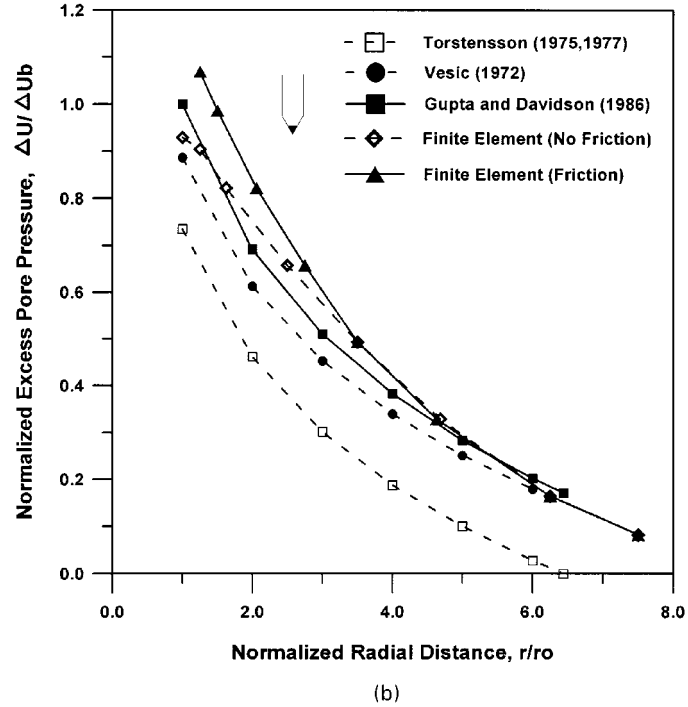

(b)

Figure 14. Spatial excess pore pressure distributions for specimen 1: (a) at the cone base, (b) at the cone tip

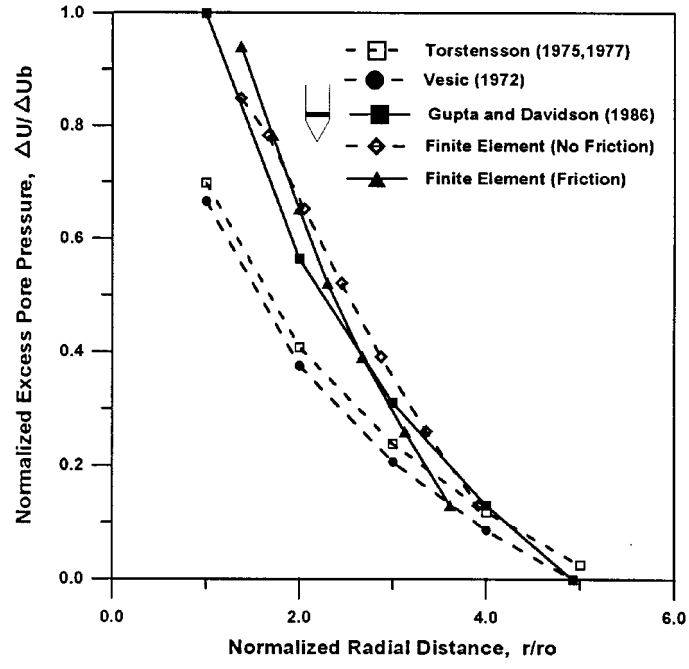

(a)

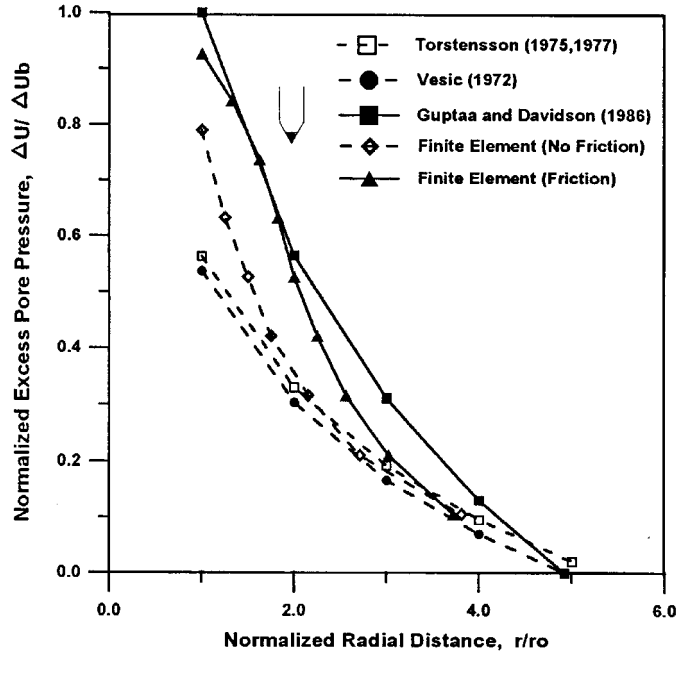

(b)

Figure 15. Spatial excess pore pressure distributions for specimen 2: (a) at the cone base, (b) at the cone tip

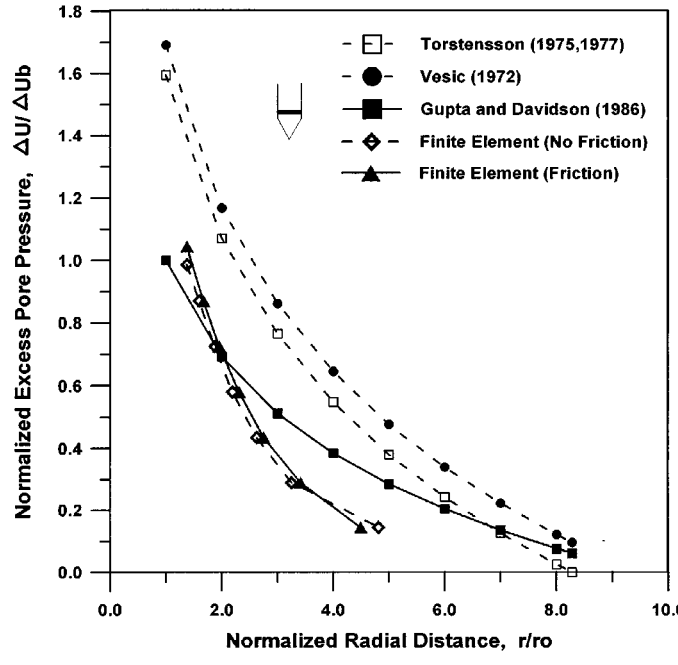

(a)

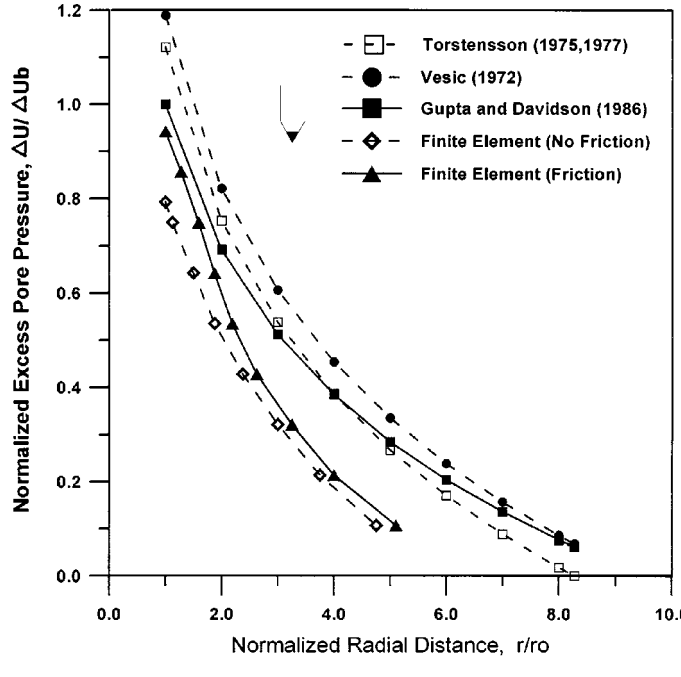

(b)

Figure 16. Spatial excess pore pressure distributions for specimen 3: (a) at the cone base, (b) at the cone tip

Table VI. Reference Soil Parameters[25]

Specimen no.	Sleeve friction f_{5pts} (kPa)	Undrained shear strength S_u (kPa)	A_f	Rigidity index $I_r = G_{50}/S_u$	Radial coefficient of consolidation ($C_r \times 10^{-3}$ cm^2/s)	
					Virgin	Reload
1	13	60	1·10	267	14·1	78·8
2	15	40	0·18	150	14·1	78·8
3	12	65	0·59	567	26·4	105·0

presents the reference soil parameters used in order to predict the spatial pore pressure distribution. These parameters are taken from the work of Kurup.[25] The spherical cavity expansion is used for both U1 and U2 configurations assuming that the penetration produces a successive spherical cavity expansion. The finite element spatial excess pore pressure distribution is quite close to that of the Gupta and Davidson[13] prediction method. The cavity expansion method proposed by Torstensson[8, 9] gives less accurate results than the other methods. This is partly due to neglecting the shear-induced excess pore pressure. Comparing the proposed method with the other prediction methods, one finds that the proposed computational method gives better and closer results to the experimental ones for specimens 1 and 2 than for the K_0-anisotropic consolidated specimen 3. The authors believe that the value of the rigidity index $I_r = G/S_u = 567$ (Reference 25) for specimen 3 is overestimated compared to the other two specimens as well as compared to the variation in the undrained shear strength, S_u, in which, G is the shear modulus. Despite the fact that some of these prediction methods may give a reasonable distribution, the proposed method using the finite element analysis has more advantages over these methods in its capability to simulate the piezocone advance during penetration process, and the incorporation of large deformation theory, soil nonlinearity and the elasto-plastic soil behavior. It also provides the spatial excess pore pressure distribution at any depth during the piezocone penetration.

Dissipation of the excess pore pressure

The dissipation results obtained numerically of the excess pore pressure with time, are compared with those obtained from the PCPT for U1 and U2 configurations as shown in Figures 17–19 for specimens 1, 2, and 3, respectively. It is obvious that both the finite element analytical results and those obtained experimentally are quite close with the exception of the absence of the sudden drop in the pore pressure at the instant that the penetration is ceased as is observed experimentally. Figures 17–19 also present the comparison between the dissipation of the excess pore pressure obtained numerically with those predicted using Torstensson's[8, 9] spherical cavity expansion model and the strain path methods proposed by Levadoux and Baligh[12] and Teh and Houlsby.[15] Teh and Houlsby introduced a modified time factor, T^*, defined as

$$T^* = (c_r t)/(r_0^2 \sqrt{I_r}) \tag{4}$$

to account for the influence of the rigidity index I_r, and the radius of the influenced zone. In equation (4), c_r is the radial coefficient of consolidation and t is the time. The equation also unifies the dissipation results for different I_r values. The finite element numerical dissipation results

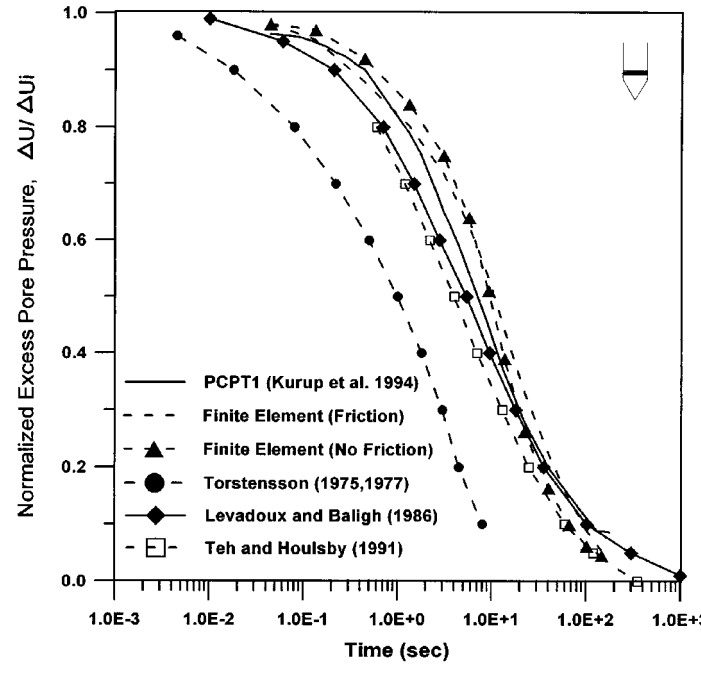

(a)

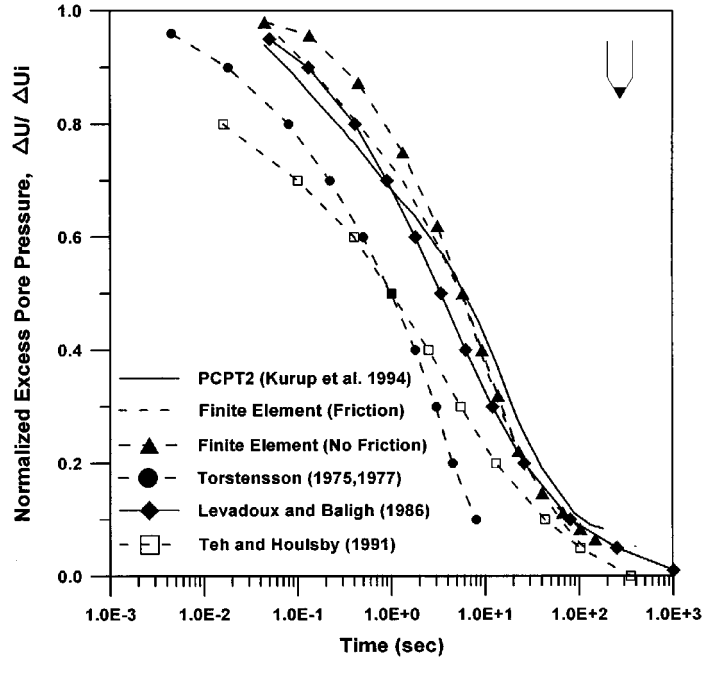

(b)

Figure 17. Dissipation of excess pore pressures for specimen 1: (a) at the cone base, (b) at the cone tip

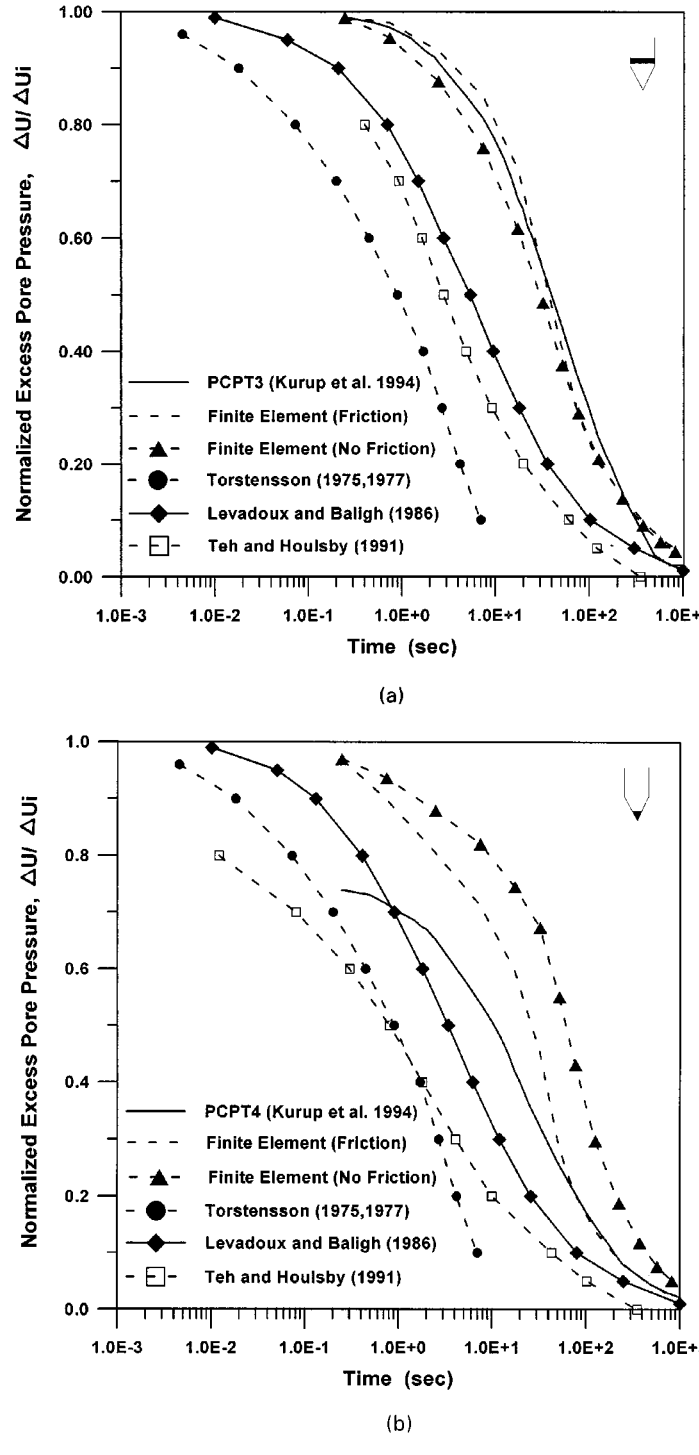

Figure 18. Dissipation of excess pore pressures for specimen 2: (a) at the cone base, (b) at the cone tip

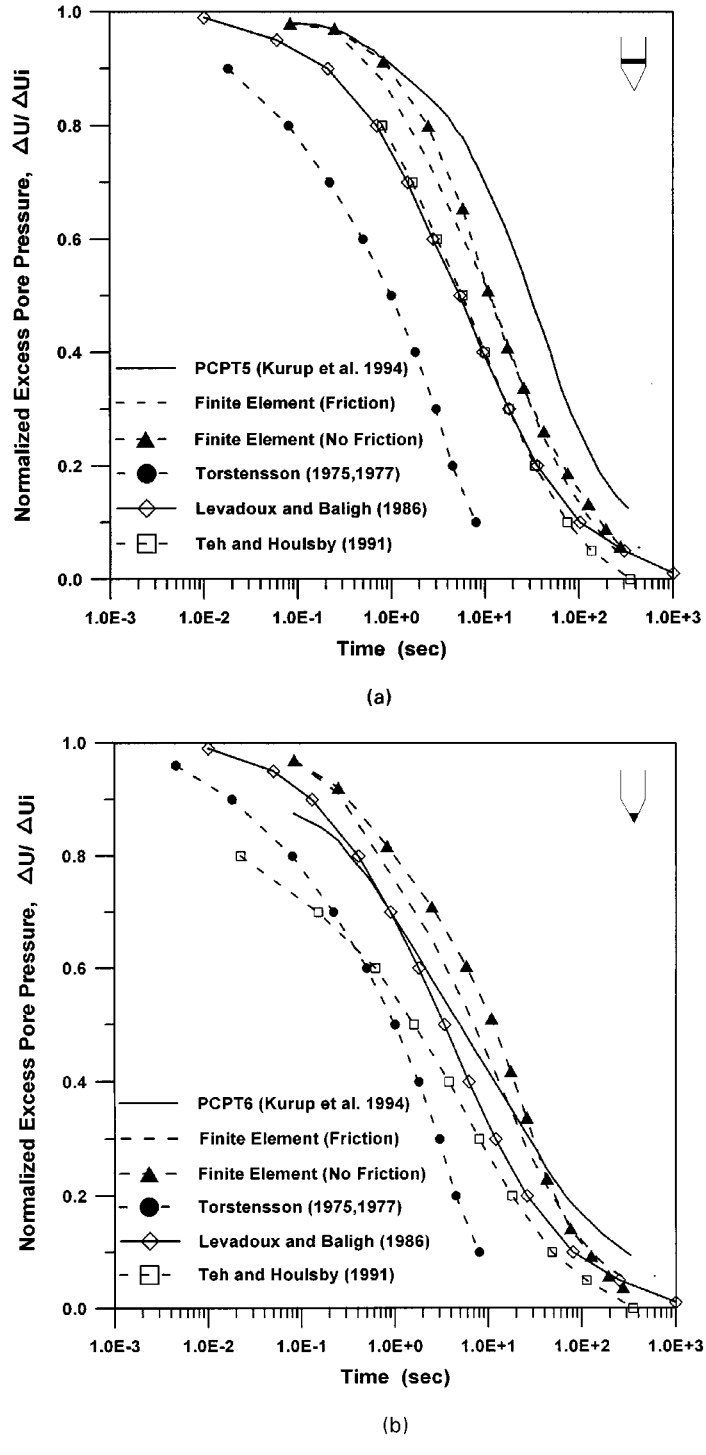

Figure 19. Dissipation of excess pore pressures for specimen 3: (a) at the cone base, (b) at the cone tip

obtained in this proposed work are closer to the results of the strain path model proposed by Levadoux and Baligh.[12] However, Levadoux and Baligh's strain path method does not indicate any significant difference between the dissipation rates at the cone tip and the cone base. The Torstensson[8, 9] cavity expansion solution gives a faster dissipation rate of the excess pore pressure than the experimental dissipation results and those dissipation results obtained numerically and theoretically using other methods.

CONCLUSIONS

An analytical model to simulate the penetration of the piezocone penetrometer in cohesive soils is presented in this paper and used in the analysis of the miniature peizocone penetration tests (PCPT) conducted at LSU/CALCHAS. Analysis is performed for different soil specimens with different stress histories. Results obtained from the numerical simulations are compared with those obtained from the miniature piezocone penetration tests (PCPT) performed on cohesive soil specimens conducted in the LSU calibration chamber. The resulting excess pore pressure distribution and its dissipation are also compared with a number of different available interpretation methods. There is a good correlation between the analytical results obtained here using the proposed method and those obtained experimentally, as well as, other interpretation methods. The following conclusions can be made from this study.

The cone tip resistance and excess pore pressure profiles obtained numerically reach a steady state condition (for the three specimens) at a penetrometer depth of 20–30 mm, which is faster than those obtained experimentally. However, the numerical value for the steady-state condition are quite close to those obtained experimentally at the steady-state condition. The calibration chamber tests usually take the 'steady-state' value as a single measurement. The difference may be due to some boundary effects and/or saturation difficulties in the experimental procedure near the top surface of the soil specimen and also due to pre-stress problems.

The stress changes induced from the piezocone penetration are quite high, and concentrated very close to the conical surface extending radially in a very small localized zone. The extent of the affected zone (with $\tau_{oct} > 10\,\text{kPa}$) is the smallest for the case of the overconsolidated specimen ($2r_0$–$3r_0$) followed by the K_0-anisotropically consolidated specimen ($3r_0$–$4r_0$) and finally by the normally consolidated specimen ($4r_0$–$5r_0$). This makes the piezocone penetration problem very localized into a small zone around the conical surface which may lead to incorrect interpretation and calculation of the soil properties and parameters due to the high stress redistribution in the area immediately around the cone tip.

The resulted excess pore pressures deviate by (10–15 per cent) due to the soil-penetrometer interface friction. This is because the soil around the piezocone is subjected to more shearing and hence, the contribution of the shear induced excess pore pressure will affect the total excess pore pressures. This is more obvious for the U1 configuration of the filter location.

A large pore pressure gradient is developed around the piezocone base especially for the overconsolidated specimen. This makes the measurement of the excess pore pressure in this zone to be highly sensitive to the filter location. Therefore, in order to avoid possible erroneous measurements, it will be better to place the transducer or filter at the middle-third of the piezocone face since this area represents the average excess pore pressures that is more uniform and less sensitive to filter location.

The radial distribution of the excess pore pressure obtained numerically is closer to that predicted using the Gupta and Davidson[13] method. The cavity expansion model proposed by

Torstensson[8,9] gives less accurate results than the other methods due to ignoring the shear induced excess pore pressures.

The dissipation results obtained numerically are quite close to those obtained experimentally and to those predicted using the strain path method proposed by Levadoux and Baligh.[12] The Torstensson's spherical cavity expansion model gives a faster dissipation rate than both the experimental and numerical dissipation results.

ACKNOWLEDGEMENTS

This research was supported by the National Science Foundation under grant MSS-9312707. The authors wish to acknowledge the support and encouragement of Dr. Priscilla P. Nelson, Program Director of G3S/CMS, Directorate for Engineering, NSF. Partial support of the Louisiana Transportation Research Center under Task Order No. 736-99-0293 is acknowledged.

REFERENCES

1. G. Z. Voyiadjis and M. Y. Abu-Farsakh, 'Coupled theory of mixtures for clayey soils', *Comput. Geotech.* **20,** 195–222 (1997).
2. P. U. Kurup, G. Z. Voyiadjis and M. T. Tumay, 'Calibration chamber studies of piezocone test in cohesive soils', *J. Geotech. Engng.* **120,** 81–107 (1994).
3. P. D. Kiousis, G. Z. Voyiadjis and M. T. Tumay, 'A large strain theory and its application in the analysis of the cone penetration mechanism', *Int. J. Numer. Analyt. Meth. Geomech.* **12,** 45–60 (1988).
4. M. T. Tumay, Y. B. Acar, E. Deseze and R. Yilmaz, 'Soil exploration in soft clays with the quasi-static electric cone penetrometer', *Proc. 2nd European Symp. on Penetration Testing* (*ESOPT* II), Vol. 2, 1982, pp. 915–921.
5. M. M. Baligh, A. S. Azzouz, Z. A. E. Wissa, R. T. Martin and J. J. Morrison, 'The piezocone penetrometer', in R. M. Norris and R. D. Holtz (eds), *Cone Penetration Testing and Experience*, ASCE, New York, NY, 1981, pp. 247–263.
6. P. W. Mayne, F. H. Kulhawy and J. N. Kay, 'Observations on the development of pore-water stresses during piezocone penetration in clay', *J. Canad. Geotech. Engng.* **27,** 418–428 (1990).
7. G. G. Meyerhof, 'The ultimate bearing capacity of wedge-shaped foundation', *Proc. 5th Int. Conf. on Soil Mechanics and Foundations*, Vol. 2, 1961, pp. 103–109.
8. B. A. Torstensson, 'Pore pressure sounding instrument', *Proc. ASCE Spec. Conf. on In-Situ Measurement of Soil Properties*, Vol. II, ASCE, New York, NY, 1975, pp. 48–54.
9. B. A. Torstensson, 'The pore pressure probe', *Paper 34*, Geotechnical Meeting, Norwegian Geotechnical Society, Oslo, Norway, 1977, pp. 34.1–34.15.
10. A. S. Vesic, 'Expansion of cavities in infinite soil mass', *J. Soil Mech. ASCE* **98,** 265–290 (1972).
11. M. M. Baligh, 'The strain path methods', *J. Geotech. Engng. ASCE* **111,** 11-8–1136 (1985).
12. J. N. Levadoux and M. M. Baligh, 'Consolidation after piezocone penetration. I: prediction', *J. Geotech. Engng. ASCE* **112,** 707–726 (1986).
13. R. C. Gupta, and J. L. Davidson, 'Piezoprobe determination coefficient of consolidation', *Soils Found.* **26,** 12–22 (1986).
14. D. Elsworth, 'Analysis of piezocone dissipation data using dislocation methods', *J. Geotech. Engng. ASCE* **119,** 1601–1623 (1993).
15. C. I. Teh and G. T. Houlsby, 'An analytical study of the cone penetration test in clay', *Geotechnique* **41,** 17–34 (1991).
16. G. Z. Voyiadjis, P. U. Kurup and M. T. Tumay, 'Preparation of large size cohesive specimens for calibration chamber testing', *Geotech. Testing J. ASTM*, **16,** 339–349 (1993).
17. M. G. Katona, 'A simple contact-friction interface element with applications to buried culverts', *Int. J. Numer. Analyt. Meth. Geomech.* **7,** 371–384 (1983).
18. O. Z. Zienkiewicz *et al.*, 'Analysis of nonlinear problems with particular reference to jointed rock systems', *Proc. 2nd Int. Conf. Society of Rock Mechanics*, Belgrade, Vol. 3, 1970, pp. 501–509.
19. X. Y. Lei, G. Swoboda and G. Zenz, 'Application of contact–friction interface element to tunnel excavation in faulted rock', *Comput. Geotech.* **17,** 349–370 (1995).
20. R. E. Goodman, R. L. Taylor and T. L. Brekke, A model for the mechanics of jointed rock', *J. Soil Mech. Found. Div. ASCE* Vol. 94, No. SM3, 637–659 (1968).
21. C. S. Desai, M. M. Zaman, J. G. Lightner and H. J. Siriwardane, 'Thin layer element for interfaces and joints', *Int. J. Numer. Analyt. Meth. Geomech.* **8,** 19–43 (1984).

22. K. G. Sharma and C. S. Desai, 'Analysis and implementation of thin-layer element for interfaces and joints', *J. Engng. Mech. ASME* **118,** 2442–2462 (1992).
23. W. F. Chen, *Limit Analysis and Soil Plasticity*, Elsevier, Amsterdam, 1975.
24. W. F. Chen and E. Mizuno, *Nonlinear Analysis in Soil Mechanics: Theory and Implementation*, Elsevier, New York, NY 1990.
25. P. U. Kurup, 'Calibration chamber studies of miniature piezocone penetration tests in cohesive soil specimens', *Ph.D. Dissertation*, Department of Civil and Environmental Engineering, Louisiana State University, LA, 1993, 258 pp.

